Article

Current Biology

Threshold-Based Ordering of Sequential Actions during *Drosophila* Courtship

Graphical Abstract

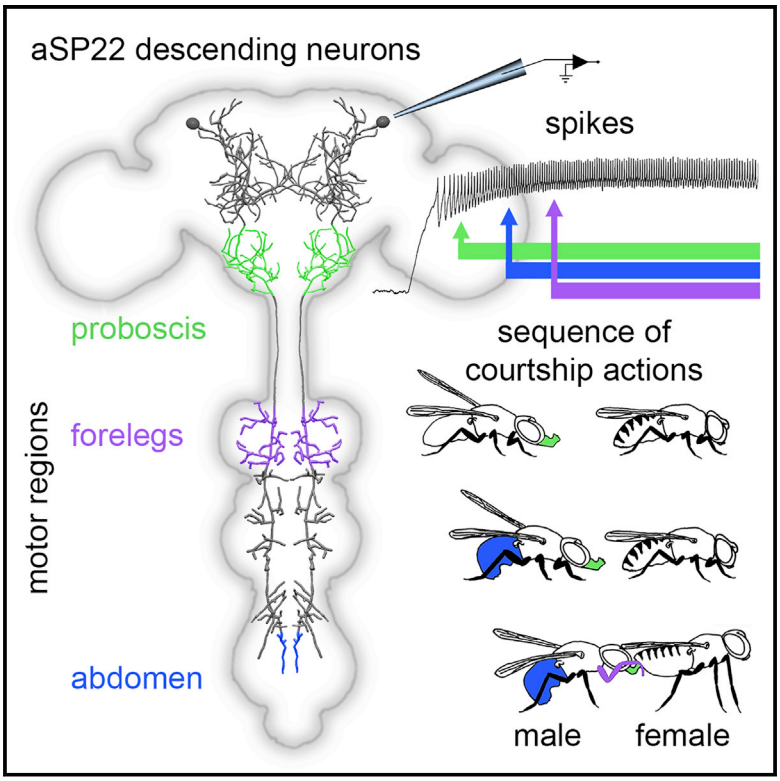

Highlights

- A descending neuron, aSP22, controls multiple actions in *Drosophila* male courtship
- aSP22 activation triggers these actions in the same sequence as found in courtship
- The courtship actions are sequenced by a ramp-to-threshold mechanism
- Distinct action thresholds are best explained by spike count, not spike frequency

Authors

Claire E. McKellar, Joshua L. Lillvis, Daniel E. Bath, James E. Fitzgerald, John G. Cannon, Julie H. Simpson, Barry J. Dickson

Correspondence

jhsimpson@ucsb.edu (J.H.S.), dicksonb@janelia.hhmi.org (B.J.D.)

In Brief

McKellar et al. show that *Drosophila* courtship includes a stereotyped behavioral motif consisting of several overlapping actions. These multiple actions are controlled by a single pair of sexually dimorphic descending neurons. These neurons elicit each successive action at progressively higher threshold spike counts.

McKellar et al., 2019, Current Biology *29*, 426–434
February 4, 2019
https://doi.org/10.1016/j.cub.2018.12.019

CellPress

CellPress

Current Biology
Article

Threshold-Based Ordering of Sequential Actions during *Drosophila* Courtship

Claire E. McKellar,[1,3] Joshua L. Lillvis,[1] Daniel E. Bath,[1,4] James E. Fitzgerald,[1] John G. Cannon,[1,5] Julie H. Simpson,[1,6,*] and Barry J. Dickson[1,2,7,*]

[1]Janelia Research Campus, Howard Hughes Medical Institute, 19700 Helix Drive, Ashburn, VA 20147, USA
[2]Queensland Brain Institute, University of Queensland, St Lucia, QLD 4072, Australia
[3]Present address: Princeton Neuroscience Institute, Washington Road, Princeton, NJ 08540, USA
[4]Present address: Department of Collective Behavior, Max Planck Institute for Ornithology, Konstanz, Germany
[5]Present address: 291 Campus Drive, Stanford, CA 94305, USA
[6]Present address: Molecular Cell and Developmental Biology, University of California, Santa Barbara, Santa Barbara, CA 93106, USA
[7]Lead Contact
*Correspondence: jhsimpson@ucsb.edu (J.H.S.), dicksonb@janelia.hhmi.org (B.J.D.)
https://doi.org/10.1016/j.cub.2018.12.019

SUMMARY

Goal-directed animal behaviors are typically composed of sequences of motor actions whose order and timing are critical for a successful outcome. Although numerous theoretical models for sequential action generation have been proposed, few have been supported by the identification of control neurons sufficient to elicit a sequence. Here, we identify a pair of descending neurons that coordinate a stereotyped sequence of engagement actions during *Drosophila melanogaster* male courtship behavior. These actions are initiated sequentially but persist cumulatively, a feature not explained by existing models of sequential behaviors. We find evidence consistent with a ramp-to-threshold mechanism, in which increasing neuronal activity elicits each action independently at successively higher activity thresholds.

INTRODUCTION

Work in multiple species has led to several theories of how nervous systems organize sequences of motor actions to form complex behaviors [1–10]. Nevertheless, evidence to support these theories has often been correlational; in few systems have specific cell types been discovered to be both necessary and sufficient for the execution of a behavioral sequence, partially due to the historical difficulty of controlling individual cell types. New genetic reagents are now allowing precise targeting of neuron types, and are particularly useful in *Drosophila melanogaster* [11], in which stereotyped neural circuits and a less numerically complex nervous system can simplify the search for neurons causal to a behavior.

A promising behavior for the search for control neurons is *Drosophila* male courtship. Males perform several motor actions such as following, wing song, proboscis extension for licking the female, tapping with the legs, and bending the abdomen for copulation [12]. Certain sequential relationships have been observed between these actions at relatively coarse timescales [13, 14], but leave open the behavioral rules that organize actions over shorter timescales. Moreover, whereas considerable progress has been made in mapping the neural circuits underlying courtship, including the control of one specific motor action (wing song [15]), it remains unclear how multiple actions are coordinated during courtship behavior.

Wing song is controlled by a command-like neuron pair (pIP10) that descends from the brain to the wing motor region [15]. Other actions might similarly be controlled by dedicated descending pathways, with parallel pathways for different actions linked by upstream circuitry that imposes temporal organization. This concept of distinct, parallel neural pathways controlling each action of a behavior is common in theories of behavioral sequencing [1, 3, 4, 9]. In search of such descending controls for courtship actions, we discovered, however, that several courtship actions are organized in a different manner.

Here, we identify a pair of descending neurons, the aSP22 neurons, that control not one but several courtship actions. We find that these courtship actions are structured differently from other behavioral sequences modeled to date, in that they are not mutually exclusive actions but overlap and persist cumulatively. Each is elicited at a different activation threshold, consistent with a ramp-to-threshold sequencing model proposed in 1960 but not heretofore investigated experimentally [14]. These findings demonstrate an alternative way for the nervous system to organize complex behavior, providing a foundation to seek analogous mechanisms and circuits in higher animals.

RESULTS

aSP22 Descending Neurons Control Multiple Courtship Actions

To explore the coordination of courtship actions, we sought to identify descending neurons involved in particular steps of male courtship. Because courtship behaviors differ between males and females, critical neurons might be sexually dimorphic in shape or function. We screened GAL4 [16, 17] and split GAL4 [16, 18, 19] driver lines genetically targeting different sets of neurons, and discovered a sexually dimorphic descending neuron pair we termed the aSP22 neurons (Figure S1; STAR Methods).

Optogenetic stimulation of aSP22 neurons with CsChrimson [20] elicited proboscis extension (Video S1), more potently in males than females (Figure 1A). Ablating aSP22 impaired proboscis extension during courtship (Figure 1B) but not during feeding (Figure 1C). Thus, at first glance, aSP22 neurons might be considered command neurons for courtship licking, analogous to the function of pIP10 neurons in generating wing song [15]. However, aSP22 neurons have extensive arborizations, with synaptic outputs in motor areas not only for the proboscis but also for the legs and abdomen (Figures 1D–1H). We thus speculated that aSP22 might be more multifunctional than the initial behavioral experiments suggested.

We did not initially notice any effect of aSP22 activation on the legs and abdomen. Any optogenetically triggered movements of these body parts might, however, have been obscured by their high frequency of spontaneous movement in freely walking flies. We found that such movements are rare in tethered, flying flies. Although this is not the natural state for courtship in *D. melanogaster*, the fact that the legs and abdomen are held relatively motionless in this preparation provided a unique opportunity to reliably detect any movements of these body parts that might result from activation of aSP22. Indeed, in this assay, a surprising number of movements were now detectable upon aSP22 stimulation: not only proboscis extension (Figure 1I) but also abdomen bending (a highly penetrant but small movement with a mean angle of ~5°; Figure 1J) and two types of leg movements, simultaneous movement of all six legs (possibly related to a postural adjustment; Figures 1K and S2A) and lifting of the forelegs in front of the head (Figure 1L; also see Videos S1, S2, and S3). These phenotypes occurred with either of two different sparse split GAL4 driver lines that each contain aSP22 but no other shared cells, *aSP22-SS1* and *-SS2* (Figures 1I–1L and S1J–S1N; STAR Methods).

As in proboscis extension, sexual dimorphism was also observed in the abdomen and leg movements triggered by aSP22 activation. In males, the abdomen showed flexion (bending), whereas in females it showed a small degree of extension rather than flexion (Figure 1J). (Note that females do not naturally perform the deep abdomen bending observed in male courtship, and that the large size of the female abdomen may constrain bending.) Foreleg lifting was more penetrant in males than females (Figure 1L). Wing extension was never elicited by aSP22 activation, in this or any other preparation (data not shown).

Not only was aSP22 sufficient to elicit these actions, it was also necessary for their normal performance in courtship. Just as proboscis extension during courtship was impaired by aSP22 ablation, so were foreleg lifting and abdomen bending (Figures 1M and 1N). The quantification of these phenotypes was made possible by a new high-resolution courtship assay using two cameras to monitor body parts at all times. Foreleg lifting had not been previously quantified, but in this assay was clearly distinguishable as a step in late-stage courtship wherein males lift both forelegs to reach under the female (Video S2), possibly positioning her for a copulation attempt. The high-resolution assay also revealed previously undescribed postural movements in courtship (not quantified; STAR Methods; Video S2). Altogether, the ablation experiments revealed that aSP22 has critical roles in at least three courtship actions (proboscis extension, leg lifting, and abdomen bending), and that these resemble the phenotypes triggered by aSP22 stimulation. Other actions were not impaired by aSP22 ablation, demonstrating the specificity of aSP22's role; wing extensions were slightly reduced, but the effect was significant only compared to one of two negative controls (Figure 1O). Courtship following, locomotion, and copulation latency were unaffected (Figures S2B–S2E).

A Recurring Engagement Motif in Male Courtship Behavior

If one neuron pair influences multiple specific actions of courtship, we might expect those actions to be temporally linked in the natural behavior. Previous efforts to characterize courtship sequences used low-resolution measurements or scored movements only of a certain size [13, 14]. Despite progress with several examples of machine vision courtship tracking [21–24], no published tracker can yet detect the earliest onset of every courtship action. For example, the proboscis first starts to extend below the head, and so could not be detected from above until it extends far enough to be observed outside the outline of the head. More importantly, machine vision tools have not yet been used to track every body part used in courtship [25]. We therefore scored the precise onsets and durations of several actions manually in courtship sequences recorded using the high-resolution two-camera video system. This analysis revealed that courtship actions can overlap extensively and that there is a non-random sequence to their initiations (Figures 2A–2D). We calculated transition probabilities between action onsets and used permutation tests to determine which transitions occurred significantly more often than predicted by chance, given the frequency of each action (Figure S3). Overrepresented transitions highlighted a stereotyped sequence of three actions: proboscis extension, followed by abdomen bending, then foreleg lifting (Figures 2D and S3A)—all actions that involve aSP22. These actions occurred as the male approached the female (Video S2), and so we termed them the "engagement" motif, in contrast to pursuit behaviors such as following and wing extension. The engagement sequence was detectable whether "self-transitions" (re-initiations of an action that had just terminated) were included (Figures 2D and S3A) or excluded (Figures S3B and S3D). Within engagement "bouts" (defined in STAR Methods), the action sequence was highly stereotyped, with transition probabilities of 0.87 from proboscis to abdomen and 0.59 from abdomen to legs (Figure S3C).

In the analysis of transitions between courtship actions, the only overrepresented transitions other than the transitions between engagement actions were self-transitions (Figures 2D and S3A). In particular, following and wing extension are frequent, repetitive behaviors (Figure 2A; bout numbers in Figures 3A and S3A). When these self-transitions were excluded from the analysis, three additional transitions were statistically overrepresented: from either following or wing extension to proboscis extension (the start of the engagement sequence), and from leg lifting (the end of the engagement sequence) to following (Figure S3B). Therefore, excluding self-transitions, a sequence of courtship actions is revealed that typically begins with following or wing extension, progresses through the engagement sequence, and then returns to following (Figure S3D).

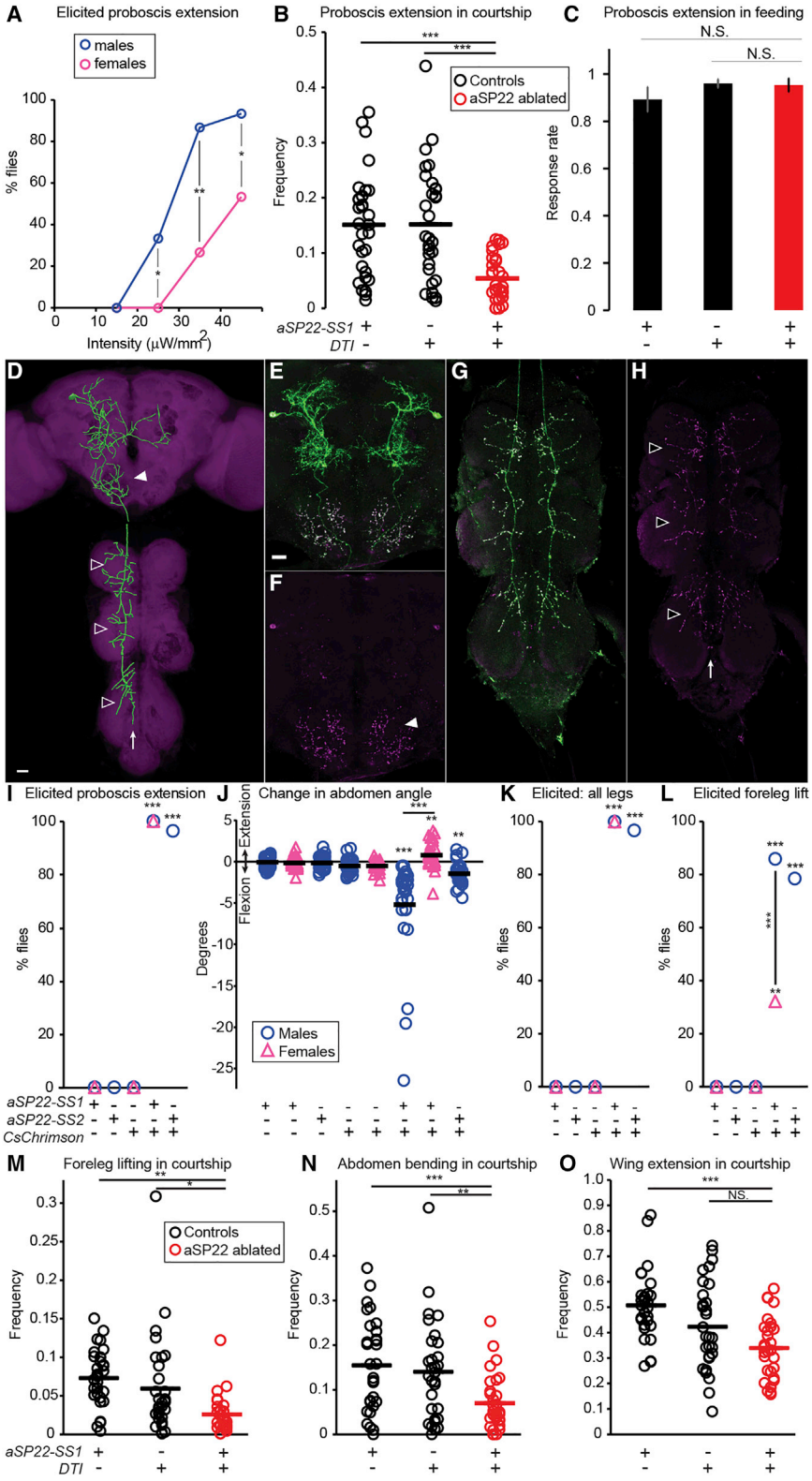

Figure 1. aSP22, a Descending Neuron Pair with Multiple Roles in Courtship

(A) Percentage of males (blue) and females (pink) showing proboscis extension upon stimulation of *aSP22-SS1* with *CsChrimson* in an open-field assay. Controls lacking *aSP22-SS1* or *CsChrimson*: no proboscis extension (not shown). n = 15 flies/condition.

(B) In a courtship assay, frequency of proboscis extension in males with aSP22 ablated with diphtheria toxin (DTI) (red) or controls (black). n = 30 males/genotype. Bars indicate the mean.

(C) Mean ± SEM. Fraction of feeding trials showing proboscis extension in response to sucrose. n = 30/genotype.

(D) Male brain (top) and ventral nervous system (VNS; bottom) with traced aSP22 (green), projecting to motor regions for proboscis (filled arrowhead), legs (open arrowheads), and abdomen (arrow). Magenta: neuropil (nc82 antibody).

(E–H) Confocal substacks of an *aSP22-SS1* male brain (E and F) and VNS (G and H), stained for membrane (green, E and G) and synaptic terminals (magenta, F and H). Scale bar, 20 μm.

(I–L) Tethered, flying aSP22 lines activated at 200 μW/mm^2 with *CsChrimson* versus controls elicited proboscis extension (I), abdomen bending (J), simultaneous movement of all legs (K), and foreleg lifting (L). n = 28 flies/genotype.

(M–O) In courtship, frequency of foreleg lifting (M), abdomen bending (N), and wing extension (O) in DTI-ablated aSP22 versus controls. n = 30 males/genotype.

Fisher's exact test or Mann-Whitney, with multiple testing correction. *p < 0.05, **p < 0.01, ***p < 0.001; N.S., not significant. See also Figures S1 and S2 and Videos S1 and S2.

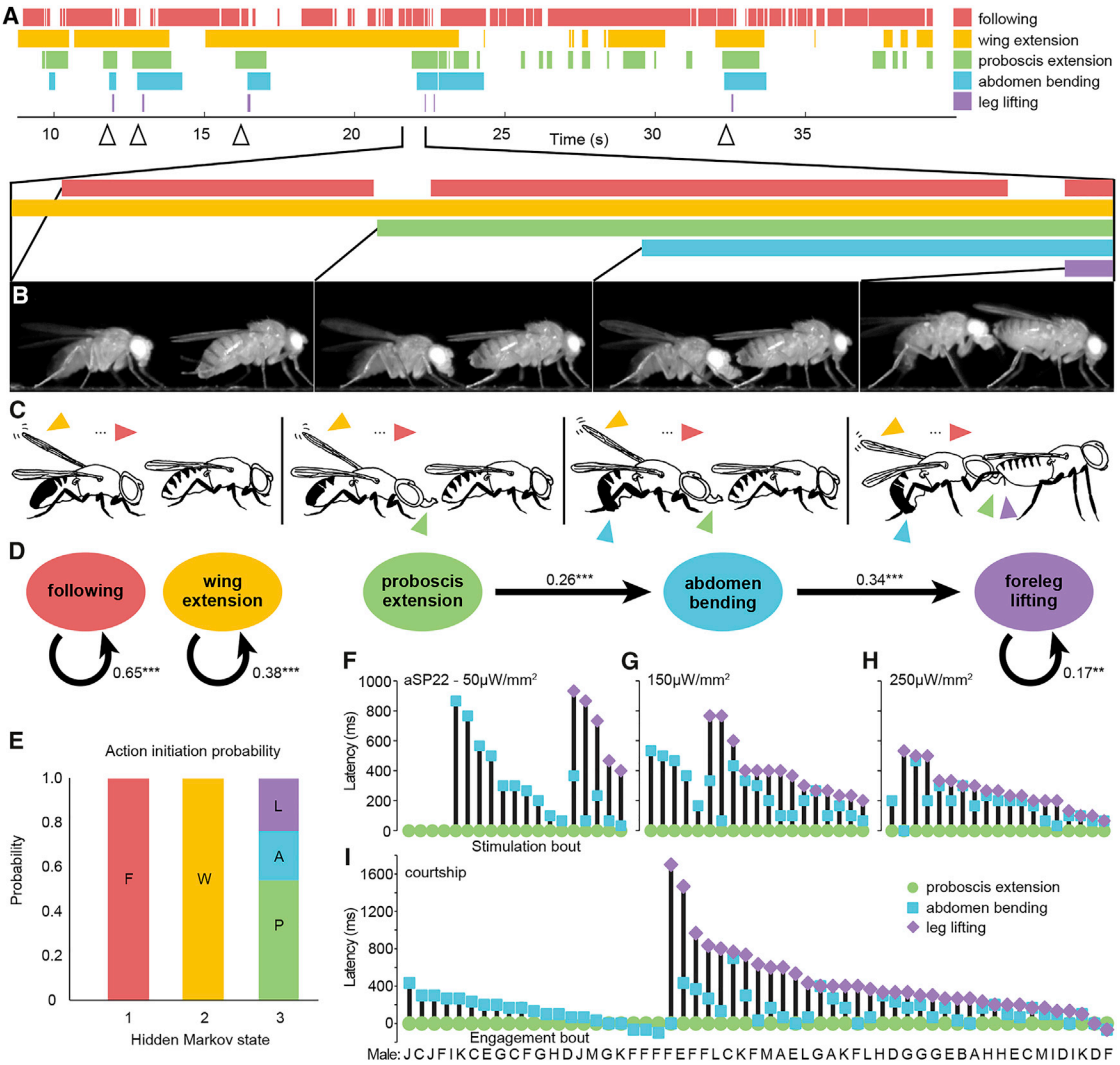

Figure 2. A Sequence of "Engagement" Actions, in Natural Courtship and upon aSP22 Activation

(A) Ethogram of a male's actions in a representative period of courtship. Arrowheads and magnified: engagement sequences.

(B and C) Video frames (B) and drawings (C) showing behaviors added cumulatively as courtship progresses. In each, male on the left and female on the right.

(D) Transitions between action onsets (including self-transitions) are significantly more frequent than predicted by overall frequency of subsequent action. n = 13 wild-type males scored at 30 frames/s (fps) for 900 frames or to copulation. **p < 0.01, ***p < 0.001.

(E) Probabilities of initiating each action in a three-state hidden Markov model.

(F–H) Action latencies from proboscis extension during stimulation of flying *aSP22-SS1>CsChrimson* males at 50 μW/mm^2 (F), 150 μW/mm^2 (G), and 250 μW/mm^2 (H). Columns: 19 individuals (1 bout/fly), ordered by strength of response.

(I) Latencies in bouts of two or more overlapping engagement actions in wild-type courtship. Columns: 57 bouts from 13 males labeled A–M.

See also Figure S3 and Videos S2 and S3.

Because transitions between engagement actions, but not to other actions, were more likely than predicted by chance (Figure S3A), we hypothesized that engagement steps could be summarized by a single kinetic state. Fitting a three-state hidden Markov model to the observed sequence of action onsets assigned both following and wing extension to single states, but the three engagement actions were grouped into a common state (Figure 2E). In other words, given the occurrence of an engagement action, the occurrence of another engagement action is more likely than the occurrence of a non-engagement action, consistent with the idea that engagement actions are under common neural control. Non-engagement actions do not cluster this way.

Having established that aSP22 activity can elicit each of the engagement actions in tethered flies, we next examined whether it was also sufficient to impart the same temporal structure to these actions observed during courtship. Indeed, aSP22 itself triggers a sequence. In isolated males, optogenetic activation of aSP22 triggered proboscis extension, then abdomen bending, then foreleg lifting, with sequential onset times (consistently ordered actions in each column of Figures 2F–2H; Video S3). This sequence was often truncated, but no action was ever

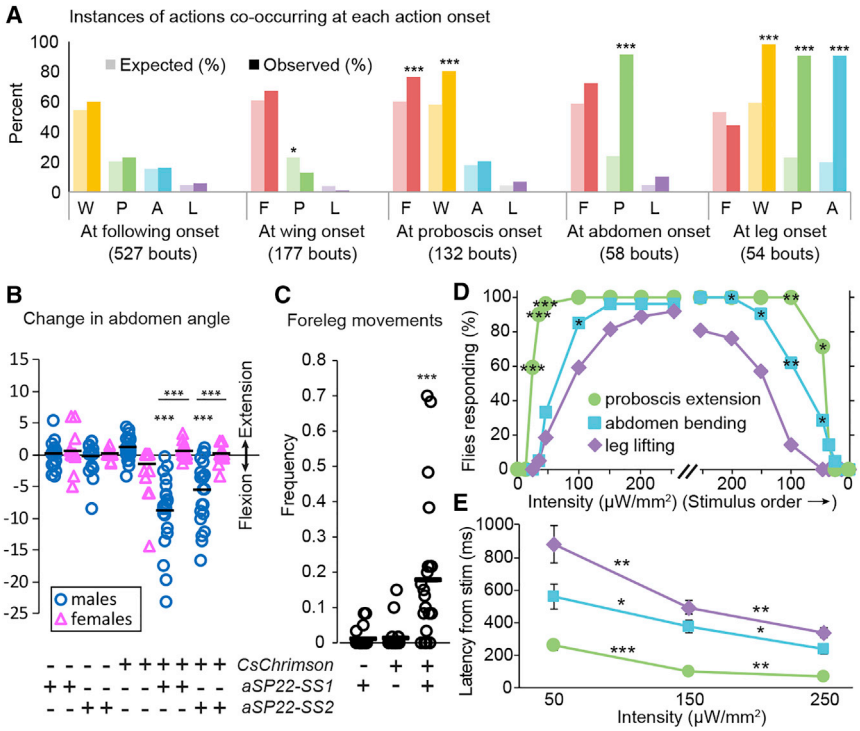

Figure 3. Testing Predictions of Models of Behavioral Sequencing

(A) Expected versus observed (defined in STAR Methods) instances of co-occurring actions at onset of each action as a percentage of onsets. F, following; W, wing extension; P, proboscis extension; A, abdomen bending; L, foreleg lifting. Omitted scoring wings during abdomen bending; contact confounds interpretation of wing movements. Fisher's exact test between expected and observed, with multiple testing correction.

(B and C) Abdomen bending (B) and foreleg movements (C) in decapitated flies stimulated at 300 μW/mm^2. n = 22 flies/condition. Mann-Whitney, reported if significantly different from both controls.

(D) In flight assay, fraction of *aSP22-SS1>CsChrimson* males performing different actions across stimuli presented in increasing (left, n = 27) or decreasing (right, n = 21) order, separated by 20-s rests. Fisher's exact test between one action and the previous. *aSP22-SS1* control and *CsChrimson* control flies (12 each): no phenotypes at any stimulus intensity (not shown).

(E) Action latency from stimulation (mean ± SEM). Mann-Whitney between one action at different intensities. *p < 0.05, **p < 0.01, ***p < 0.001; no asterisks, not significant.

skipped or out of sequence. The same fixed but sometimes truncated sequence was also seen in the engagement bouts of natural courtship (Figure 2I; individual transition probabilities in Figure S3C), albeit with slightly less stereotypy (7% [4/57] of bouts occurred out of order). When aSP22 was ablated, although engagement actions occurred less frequently (Figures 1B, 1M, and 1N), they still occurred in the same sequence (Figures S3E–S3G). Engagement is therefore partially dependent on aSP22, with other neurons most likely participating as well.

A Ramp-to-Threshold Model for Sequencing of Engagement Actions by aSP22

How might a single cell type order multiple courtship actions? Several action sequencing models, such as those proposed for behaviors including human typing [3, 26] and fly grooming [9], assume that inhibitory or competitive interactions between parallel circuits for each motor action prevent their simultaneous occurrence. Such scenarios are unlikely to apply to the actions of courtship, as they co-occur extensively (Figures 2A–2C). To quantify this overlap, we analyzed single video frames at each action onset to determine which other actions were ongoing at that time. When pursuit actions (following or wing extension) began, the co-occurrence of other actions was no more frequent than predicted by chance (Figure 3A). However, as each engagement action began, the sequentially earlier actions persisted at frequencies higher than expected by chance: at the onset of proboscis extension, following and wing extension were overrepresented; as abdomen bending began, the proboscis was still extended; and at the onset of leg lifting, the proboscis was extended and the abdomen bent. Thus, as courtship progresses into engagement, actions begin sequentially and persist cumulatively; they are not mutually exclusive. Escalating, overlapping actions are not explicitly featured in most models of sequential behavior [1–10]. Additional models based on various forms of inhibition, in mammalian striatum and fly larvae [4, 8, 10], also do not explicitly model overlapping actions, as seen here. Although more complex variants of these models might accommodate overlapping actions, we sought the simplest model that could explain our observations.

We next considered two excitatory models. In a "reflex chain," one action causes sensory feedback that stimulates the next [27]. In an "activation chain," a sequence is generated by feedforward excitation between parallel circuit elements controlling different actions [5]. Both of these models predict that removing motor circuits for the first action should prevent the second. We therefore decapitated flies to remove the proboscis and its motor circuitry. Stimulating only the remaining descending arbor of aSP22 still triggered the later two behaviors of abdomen bending and foreleg movements (Figures 3B and 3C). (In decapitated flies, just as in intact flies [Figure 1J], abdomen bending was triggered using either split GAL4 line and was sexually dimorphic [Figure 3B].) Thus, neither of these feedforward activation models can readily account for action sequencing by aSP22.

The final model that we investigated was a ramp to threshold, debated since 1960 [14, 28] but not heretofore supported experimentally. This model proposed that hypothetical central coordinating circuitry would show a ramp of activity as courtship arousal increases, which could trigger a sequence of actions if each action had a higher activation threshold. To test the predictions of the ramp-to-threshold model, we examined whether the three actions of the engagement motif are each triggered at a distinct aSP22 stimulus threshold, and whether aSP22 activity ramps during the optogenetic stimulus. We found that aSP22 activation elicited each successive action at a distinct stimulus

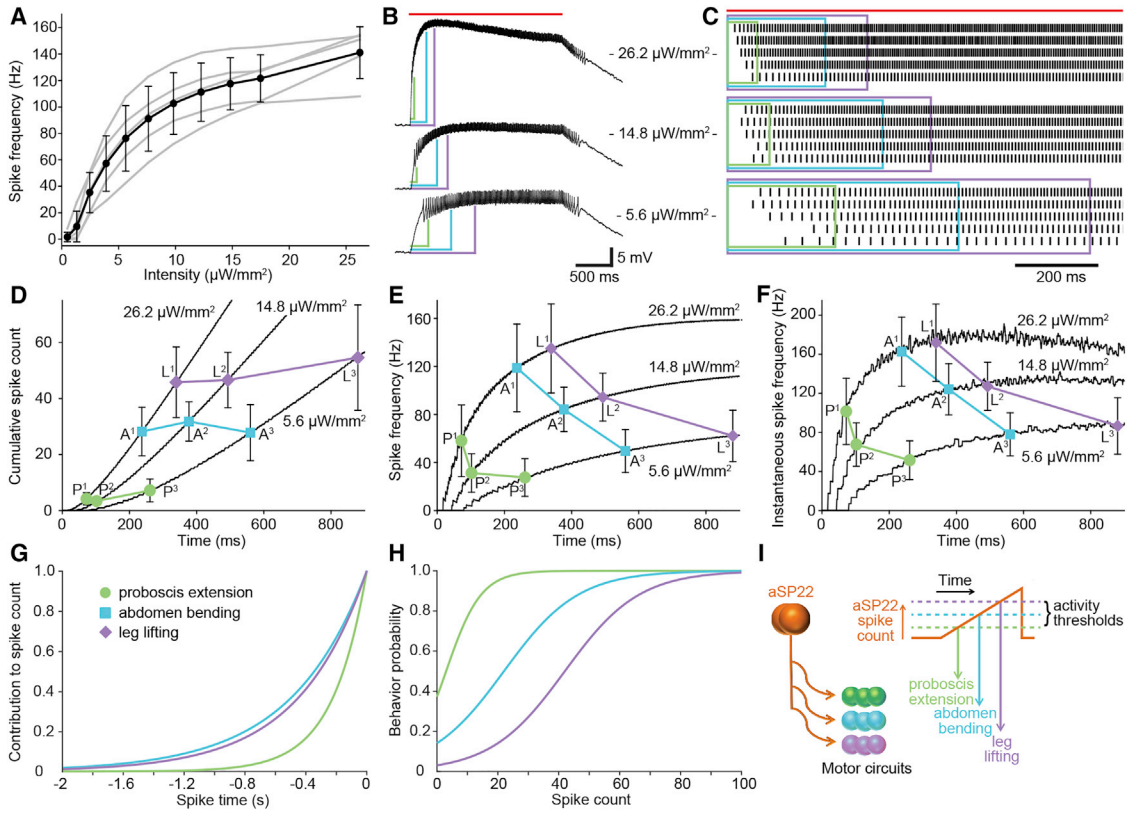

Figure 4. A Ramp-to-Threshold Mechanism Using Spike Counting for the Sequencing of Courtship Engagement Actions

(A) *Ex vivo* electrophysiology: aSP22 spike frequency during 2-s optogenetic stimuli at the intensities shown. Gray: individuals; black: mean ± SD.

(B and C) aSP22 activity in representative recordings (B) and rasters from 5 animals (C) during stimuli (red line) at three intensities, estimated to match *in vivo* intensities from Figure 3E. Colored lines (legend below): mean action latencies from behavior experiments.

(D–F) Black lines: mean cumulative spike count from stimulus onset (D), mean spike frequency from stimulus onset (E), or mean instantaneous spike frequency (F) at three intensities over time. Colors: mean ± SD of each parameter, at each behavioral latency for each intensity (as in B and C). Letters: p values in STAR Methods.

(G and H) Best-fit exponential temporal discounting functions (G) and sigmoidal activation functions (H) in a nonlinear logistic regression model fit to the measured aSP22 activity and behavior.

(I) Schematic: ramp in aSP22 activity orders the action sequence in an engagement bout.

threshold, regardless of stimulus presentation order (Figure 3D). Moreover, the activation threshold was progressively higher for successive actions (Figure 3D) and the respective latencies became shorter as the stimulus intensity increased (Figure 3E). These data suggest that a ramp-to-threshold model can best explain the ability of aSP22 to determine both the order and timing of the engagement actions.

Evidence that aSP22 Spike Counts Encode Action Thresholds

This postulated ramping activity could arise from an escalation in aSP22 spiking. In whole-cell patch-clamp recordings of *ex vivo* preparations, aSP22 spike frequency indeed ramped up over behaviorally relevant optogenetic stimulus intensities (~5–25 μW/mm^2, based on the estimate that ~10% of 630-nm light penetrates the cuticle [29]; Figures 4A and 4C) and over time periods consistent with the behavioral latencies (~100–1,000 ms). However, cumulative spike count, overall spike frequency, and instantaneous spike frequency all increased with intensity (Figures 4B and 4C) and with time (black lines, Figures 4D and 4F). If a particular one of these three spike parameters encodes action thresholds, then each action should be triggered at a consistent value for that parameter regardless of stimulus intensity. At the mean latency time for each action from behavior experiments (colored lines, Figures 4B and 4C), we calculated each spiking parameter at each stimulus intensity. Only in the case of spike count were these values consistent across varying stimulus intensities (colored lines, Figures 4D–4F). Furthermore, only the spike count values at these times were different for each action, and hence capable of encoding three distinct thresholds, at each stimulus intensity. These data suggest, surprisingly, that the threshold for each behavior is determined by cumulative aSP22 spike count, not spike frequency.

The predictions of the cumulative spike count model were reaffirmed by a nonlinear logistic regression model predicting the timing of behavioral responses from aSP22 spiking activity (STAR Methods), consistent with spikes being counted by a leaky integrator mechanism. The model uses exponential temporal discounting functions to allow recent spikes to contribute more to the spike count (Figure 4G). The best-fit parameters

predict that aSP22 spike counts are integrated with time constants of approximately 220 ms for proboscis extension, 500 ms for abdominal bending, and 450 ms for leg lifting, which suggests that single aSP22 spikes can significantly affect actions occurring on the order of a second later (Figure 4G). The model estimates the probability of each action by transforming the spike counts with sigmoidal activation functions (Figure 4H). By positing that the threshold spike count for proboscis extension is lower than that for abdomen bending, which is in turn lower than the threshold for leg lifting (Figure 4H), the model reaffirms the predictions of the cumulative spike count model (Figure 4D). Future technical advances to enable electrophysiological recordings during natural courtship will be needed to enable direct tests of how spike count controls behavior.

DISCUSSION

Our findings indicate that three distinct courtship actions are chunked together in a single behavioral motif coordinately controlled, in part at least, by the aSP22 descending neurons (Figure 4I). The frequencies of all three of these actions were reduced during courtship upon genetic ablation of aSP22. Conversely, to the extent that each engagement action can be performed or detected, it was reliably observed upon optogenetic activation of aSP22 in each of the reduced preparations we have used (isolated, freely walking males; decapitated males; tethered and suspended males).

These activation assays each have different limitations, so multiple assays were used to confirm that phenotypes were not exclusive to one assay. The tethered flight assay allowed precise timing of all three engagement actions to be measured because these body parts are held largely immobile during flight. However, flies typically court while walking, not during flight. Nonetheless, the engagement sequence of abdomen and leg movements was also triggered in standing flies, immobilized by decapitation (which also removes the proboscis), and proboscis extension was triggered in intact freely walking flies (in which any evoked movements of legs and abdomen are obscured by spontaneous locomotion). Thus, none of these aSP22-induced actions depends on the animal's locomotor state (flying or walking), nor does the sequence of at least two (and most likely all three) of these actions.

Our finding that several courtship actions are influenced by a single neuron pair is a surprising departure from a model suggested from the analysis of wing song circuitry [15], in which an action would be controlled by a dedicated descending pathway, with independent and parallel pathways for each action. In contrast, aSP22 and indeed many descending neurons have diverging projections that innervate multiple motor areas in the ventral nervous system [30]. Even the command-like neuron for wing song, pIP10, has projections to more than just the wing neuropil [15]. Because multiple descending neurons project to multiple motor neuropils, each neuron might contribute to several actions, and each action might receive input from several descending neurons. Ablating aSP22 reduces the frequency of engagement actions but does not eliminate them, suggesting that other descending neurons may act along with aSP22.

During courtship, the engagement actions are initiated in an almost invariant sequence, which is precisely recapitulated in isolated males upon activation of aSP22. Thus, aSP22 activity is not only central to the execution of each action but can account for their sequential occurrence. It is not known how multiple activation thresholds could be implemented by downstream neurons, but different input activity may be required to elicit each action due to differences in each action's circuitry or biomechanics.

A ramp-to-threshold mechanism, coded by spike count, provides a parsimonious explanation of the ordering of the engagement actions. This model offers a flexible and neurally efficient means of generating action sequences, as the actions can be sequentially evoked without any neural mechanism to ensure their mutual exclusivity or the feedforward signaling that is invoked in other models [1, 3–6, 9]. If multiple neurons each contribute spikes to be counted by downstream circuits, then eliminating just one class of input neurons would be predicted to reduce the frequency of these actions, but not change their order, as we observed upon aSP22 ablation.

The chunking and ordering of discrete actions under the ramp-to-threshold control of descending pathways may be a common mechanism to coordinate certain tightly stereotyped sequential actions of complex behaviors. We show here that sequential behaviors need not have mutually exclusive steps, as has often been assumed. Although other sequential behaviors have not yet been investigated for the type of cumulative, overlapping organization we describe, high-temporal-resolution behavioral scoring could be applied in other animals to discover analogous organization. The applicability of a ramp-to-threshold mechanism to other animals may also be supported by possible analogs of multifunctional *Drosophila* descending neurons in mammals. Corticospinal neurons in monkey, for example, descend to the spinal cord, where they branch into multiple segmental levels and project to the motor nuclei of multiple muscles [31].

Across biology, thresholds often function to organize patterns, such as an expression gradient of a morphogen eliciting different gene responses at different thresholds [32]. The present work reveals how an analogous mechanism can produce and interpret graded neural activity from a central coordinator to pattern motor actions into complex behaviors.

STAR★METHODS

Detailed methods are provided in the online version of this paper and include the following:

- KEY RESOURCES TABLE
- CONTACT FOR REAGENT AND RESOURCE SHARING
- EXPERIMENTAL MODEL AND SUBJECT DETAILS
- METHOD DETAILS
  - Identification of aSP22 neurons
  - Immunohistochemistry and image processing
  - CsChrimson activation
  - Courtship
  - Assessing postural movements
  - Feeding
  - Electrophysiology
  - Light intensity calibration
  - Logistic regression model
- QUANTIFICATION AND STATISTICAL ANALYSIS
- DATA AND SOFTWARE AVAILABILITY

SUPPLEMENTAL INFORMATION

Supplemental Information includes three figures and three videos and can be found with this article online at https://doi.org/10.1016/j.cub.2018.12.019.

ACKNOWLEDGMENTS

For fly strains, we thank Barret Pfeiffer, Heather Dionne, Gerald Rubin, Vivek Jayaraman, and Hugo Bellen. For technical support, we thank Jack Etheredge, Phuong Chung, and the Janelia Fly Core, Instrument Design & Fabrication, Project Technical Resources, Fly Light, and Scientific Computing groups. For review of the manuscript, we thank Brett Mensh, Mala Murthy, Karel Svoboda, Glenn Turner, and Marta Zlatic. This work was funded by the Howard Hughes Medical Institute.

AUTHOR CONTRIBUTIONS

Conceptualization, C.E.M., J.L.L., B.J.D., and J.H.S.; Formal Analysis, C.E.M., J.L.L., J.E.F., D.E.B., and J.G.C.; Funding Acquisition, B.J.D. and J.H.S.; Investigation, C.E.M., J.L.L., J.E.F., D.E.B., and J.G.C.; Methodology, C.E.M., J.L.L., J.E.F., and D.E.B.; Project Administration & Supervision, B.J.D., J.H.S., and C.E.M.; Visualization, C.E.M., J.L.L., J.E.F., and D.E.B.; Writing – Original Draft, C.E.M., B.J.D., J.L.L., J.E.F., and D.E.B.; Writing – Review & Editing, B.J.D., C.E.M., J.H.S., J.L.L., J.E.F., and D.E.B.

DECLARATION OF INTERESTS

The authors declare no competing interests.

Received: August 8, 2018
Revised: November 1, 2018
Accepted: December 13, 2018
Published: January 17, 2019

REFERENCES

1. Edwards, D.H. (1991). Mutual inhibition among neural command systems as a possible mechanism for behavioral choice in crayfish. J. Neurosci. *11*, 1210–1223.
2. Geddes, C.E., Li, H., and Jin, X. (2018). Optogenetic editing reveals the hierarchical organization of learned action sequences. Cell *174*, 32–43.e15.
3. Houghton, G., and Hartley, T. (1995). Parallel models of serial behavior: Lashley revisited. Psyche (Stuttg.) *2*, 1–25.
4. Jovanic, T., Schneider-Mizell, C.M., Shao, M., Masson, J.-B., Denisov, G., Fetter, R.D., Mensh, B.D., Truman, J.W., Cardona, A., and Zlatic, M. (2016). Competitive disinhibition mediates behavioral choice and sequences in *Drosophila*. Cell *167*, 858–870.e19.
5. Long, M.A., Jin, D.Z., and Fee, M.S. (2010). Support for a synaptic chain model of neuronal sequence generation. Nature *468*, 394–399.
6. Mackevicius, E.L., and Fee, M.S. (2018). Building a state space for song learning. Curr. Opin. Neurobiol. *49*, 59–68.
7. Markowitz, J.E., Gillis, W.F., Beron, C.C., Neufeld, S.Q., Robertson, K., Bhagat, N.D., Peterson, R.E., Peterson, E., Hyun, M., Linderman, S.W., et al. (2018). The striatum organizes 3D behavior via moment-to-moment action selection. Cell *174*, 44–58.e17.
8. Murray, J.M., and Escola, G.S. (2017). Learning multiple variable-speed sequences in striatum via cortical tutoring. eLife *6*, e26084.
9. Seeds, A.M., Ravbar, P., Chung, P., Hampel, S., Midgley, F.M., Jr., Mensh, B.D., and Simpson, J.H. (2014). A suppression hierarchy among competing motor programs drives sequential grooming in *Drosophila*. eLife *3*, e02951.
10. Tristan, I., Rulkov, N.F., Huerta, R., and Rabinovich, M. (2014). Timing control by redundant inhibitory neuronal circuits. Chaos *24*, 013124.
11. Venken, K.J.T., Simpson, J.H., and Bellen, H.J. (2011). Genetic manipulation of genes and cells in the nervous system of the fruit fly. Neuron *72*, 202–230.
12. Yamamoto, D., Sato, K., and Koganezawa, M. (2014). Neuroethology of male courtship in *Drosophila*: from the gene to behavior. J. Comp. Physiol. A Neuroethol. Sens. Neural Behav. Physiol. *200*, 251–264.
13. Kohatsu, S., and Yamamoto, D. (2015). Visually induced initiation of *Drosophila* innate courtship-like following pursuit is mediated by central excitatory state. Nat. Commun. *6*, 6457.
14. Manning, A. (1960). The sexual behaviour of two sibling *Drosophila* species. Behaviour *15*, 123–145.
15. von Philipsborn, A.C., Liu, T., Yu, J.Y., Masser, C., Bidaye, S.S., and Dickson, B.J. (2011). Neuronal control of *Drosophila* courtship song. Neuron *69*, 509–522.
16. Pfeiffer, B.D., Ngo, T.-T.B., Hibbard, K.L., Murphy, C., Jenett, A., Truman, J.W., and Rubin, G.M. (2010). Refinement of tools for targeted gene expression in *Drosophila*. Genetics *186*, 735–755.
17. Jenett, A., Rubin, G.M., Ngo, T.-T.B., Shepherd, D., Murphy, C., Dionne, H., Pfeiffer, B.D., Cavallaro, A., Hall, D., Jeter, J., et al. (2012). A *GAL4*-driver line resource for *Drosophila* neurobiology. Cell Rep. *2*, 991–1001.
18. Dionne, H., Hibbard, K.L., Cavallaro, A., Kao, J.-C., and Rubin, G.M. (2018). Genetic reagents for making split-GAL4 lines in *Drosophila*. Genetics *209*, 31–35.
19. Luan, H., Peabody, N.C., Vinson, C.R., and White, B.H. (2006). Refined spatial manipulation of neuronal function by combinatorial restriction of transgene expression. Neuron *52*, 425–436.
20. Klapoetke, N.C., Murata, Y., Kim, S.S., Pulver, S.R., Birdsey-Benson, A., Cho, Y.K., Morimoto, T.K., Chuong, A.S., Carpenter, E.J., Tian, Z., et al. (2014). Independent optical excitation of distinct neural populations. Nat. Methods *11*, 338–346.
21. Agrawal, S., Safarik, S., and Dickinson, M. (2014). The relative roles of vision and chemosensation in mate recognition of *Drosophila melanogaster*. J. Exp. Biol. *217*, 2796–2805.
22. Coen, P., Clemens, J., Weinstein, A.J., Pacheco, D.A., Deng, Y., and Murthy, M. (2014). Dynamic sensory cues shape song structure in *Drosophila*. Nature *507*, 233–237.
23. Kabra, M., Robie, A.A., Rivera-Alba, M., Branson, S., and Branson, K. (2013). JAABA: interactive machine learning for automatic annotation of animal behavior. Nat. Methods *10*, 64–67.
24. Ribeiro, I.M.A., Drews, M., Bahl, A., Machacek, C., Borst, A., and Dickson, B.J. (2018). Visual projection neurons mediating directed courtship in *Drosophila*. Cell *174*, 607–621.e18.
25. Robie, A.A., Seagraves, K.M., Egnor, S.E.R., and Branson, K. (2017). Machine vision methods for analyzing social interactions. J. Exp. Biol. *220*, 25–34.
26. Lashley, K.S. (1951). The problem of serial order in behavior. In Cerebral Mechanisms in Behavior, L.A. Jeffress, ed. (Wiley), pp. 112–131.
27. Clower, W.T. (1998). Early contributions to the reflex chain hypothesis. J. Hist. Neurosci. *7*, 32–42.
28. Manoli, D.S., and Baker, B.S. (2004). Median bundle neurons coordinate behaviours during *Drosophila* male courtship. Nature *430*, 564–569.
29. Inagaki, H.K., Jung, Y., Hoopfer, E.D., Wong, A.M., Mishra, N., Lin, J.Y., Tsien, R.Y., and Anderson, D.J. (2014). Optogenetic control of *Drosophila* using a red-shifted channelrhodopsin reveals experience-dependent influences on courtship. Nat. Methods *11*, 325–332.
30. Namiki, S., Dickinson, M.H., Wong, A.M., Korff, W., and Card, G.M. (2018). The functional organization of descending sensory-motor pathways in *Drosophila*. eLife *7*, e34272.
31. Shinoda, Y., Yokota, J., and Futami, T. (1981). Divergent projection of individual corticospinal axons to motoneurons of multiple muscles in the monkey. Neurosci. Lett. *23*, 7–12.
32. Wolpert, L. (1969). Positional information and the spatial pattern of cellular differentiation. J. Theor. Biol. *25*, 1–47.
33. Stockinger, P., Kvitsiani, D., Rotkopf, S., Tirián, L., and Dickson, B.J. (2005). Neural circuitry that governs *Drosophila* male courtship behavior. Cell *121*, 795–807.

34. Bellen, H.J., D'Evelyn, D., Harvey, M., and Elledge, S.J. (1992). Isolation of temperature-sensitive diphtheria toxins in yeast and their effects on *Drosophila* cells. Development *114*, 787–796.

35. Han, D.D., Stein, D., and Stevens, L.M. (2000). Investigating the function of follicular subpopulations during *Drosophila* oogenesis through hormone-dependent enhancer-targeted cell ablation. Development *127*, 573–583.

36. Nern, A., Pfeiffer, B.D., and Rubin, G.M. (2015). Optimized tools for multicolor stochastic labeling reveal diverse stereotyped cell arrangements in the fly visual system. Proc. Natl. Acad. Sci. USA *112*, E2967–E2976.

37. Jefferis, G.S.X.E., Potter, C.J., Chan, A.M., Marin, E.C., Rohlfing, T., Maurer, C.R., Jr., and Luo, L. (2007). Comprehensive maps of *Drosophila* higher olfactory centers: spatially segregated fruit and pheromone representation. Cell *128*, 1187–1203.

38. Feng, L., Zhao, T., and Kim, J. (2015). neuTube 1.0: a new design for efficient neuron reconstruction software based on the SWC format. eNeuro 2, ENEURO, 0049–14.2014.

39. Backhaus, B., Sulkowski, E., and Schlote, F.W. (1984). A semi-synthetic, general-purpose medium for *Drosophila melanogaster*. Drosoph. Inf. Serv. *60*, 210–212.

40. Yu, J.Y., Kanai, M.I., Demir, E., Jefferis, G.J., and Dickson, B.J. (2010). Cellular organization of the neural circuit that drives *Drosophila* courtship behavior. Curr. Biol. *18*, 1602–1614.

41. Ito, K., Shinomiya, K., Ito, M., Armstrong, J.D., Boyan, G., Hartenstein, V., Harzsch, S., Heisenberg, M., Homberg, U., Jenett, A., et al.; Insect Brain Name Working Group (2014). A systematic nomenclature for the insect brain. Neuron *81*, 755–765.

STAR★METHODS

KEY RESOURCES TABLE

REAGENT or RESOURCE	SOURCE	IDENTIFIER
Antibodies		
rabbit anti-DsRed	Clontech	Cat#632496; RRID: AB_10013483
mouse mAb anti-bruchpilot (nc82)	Developmental Studies Hybridoma Bank	Cat#nc82; RRID: AB_2314865
rabbit anti-GFP	Thermo Fisher Scientific	Cat#A11122; RRID: AB_221569
chicken anti-GFP	Abcam	Cat#ab13970; RRID: AB_300798
rat mAb anti-FLAG	Novus Biologicals	Cat# NBP1-06712; RRID: AB_1625981
rabbit anti-HA	Cell Signaling Technology	Cat# 3724S; RRID: AB_1549585
mouse anti-V5	AbD Serotec	Cat# MCA1360; RRID: AB_322378
rabbit anti-Fru^M	Barry Dickson [33]	N/A
goat anti-rabbit AlexaFluor-488	Thermo Fisher Scientific	Cat#A11008; RRID: AB_143165
goat anti-chicken AlexaFluor-488	Thermo Fisher Scientific	Cat#A11039; RRID: AB_142924
goat anti-mouse AlexaFluor-488	Thermo Fisher Scientific	Cat #A11001; RRID: AB_2534069
goat anti-mouse AlexaFluor-568	Thermo Fisher Scientific	Cat#A11004; RRID: AB_141371
goat anti-rat AlexaFluor-568	Thermo Fisher Scientific	Cat #A11077; RRID: AB_2534121
goat anti-rat AlexaFluor-633	Thermo Fisher Scientific	Cat#A21094; RRID: AB_141553
Chemicals, Peptides, and Recombinant Proteins		
All-trans retinal	Toronto Research Chemical	Cat# R240000
Experimental Models: Organisms/Strains		
D. melanogaster: Canton S	Bloomington Stock Center	RRID:BDSC_64349
D. melanogaster: *GMR22G01-GAL4* in attP2	Gerald Rubin [16, 17]	N/A
D. melanogaster: aSP22 split GAL4 *aSP22-SS1*	This paper; split GAL halves from Gerald Rubin [16–18]	N/A
D. melanogaster: aSP22 split GAL4 *aSP22-SS2*	This paper; split GAL halves from Gerald Rubin [16–18]	N/A
D. melanogaster: *10XUAS-IVS-mCD8::GFP* in su(Hw)attP5 (pJFRC2)	Gerald Rubin [16]	N/A
D. melanogaster: *UAS-sytGFP*	Bloomington Stock Center	Cat#6925
D. melanogaster: *pJFRC22-10xUAS-myr::tdTomato* in attP2	Bloomington Stock Center	Cat#32221
D. melanogaster: *20XUAS-CsChrimson-mCherry* in su(Hw)attP5	Insertion from Vivek Jayaraman, construct from [20]	N/A
D. melanogaster: *UAS-DTI*	Hugo Bellen [34, 35]	N/A
D. melanogaster: *pBPhsFlp2::PEST in attP3;; pJFRC201-10XUAS-FRT>STOP>FRT-myr::smGFP-HA* in VK00005	Gerald Rubin [36]	N/A
D. melanogaster: *pJFRC240-10XUAS-FRT>STOP>FRT-myr::smGFP-V5-THS-10XUAS-FRT>STOP>FRT-myr::smGFP-FLAG* in su(Hw)attP1	Gerald Rubin [36]	N/A
Software and Algorithms		
Adobe Photoshop	Adobe Systems (https://www.adobe.com/products/photoshop.html)	RRID:SCR_014199
Adobe Illustrator	Adobe Systems (https://www.adobe.com/products/illustrator.html)	RRID:SCR_010279
Computational Morphometry Toolkit	Greg Jefferis [37]	RRID:SCR_002234
LabView	National Instruments (http://www.labview.com)	RRID:SCR_014325

(*Continued on next page*)

Continued

REAGENT or RESOURCE	SOURCE	IDENTIFIER
Fiji	http://fiji.sc/	RRID:SCR_002285
neuTube	https://www.neutracing.com [38]	N/A
Matebook	Barry Dickson [24]	N/A
gVision	Gus Lott (http://gvision-hhmi.sourceforge.net/)	N/A
VCode	http://social.cs.uiuc.edu/projects/vcode.html	N/A
Spike2	Cambridge Electronic Design (http://www.ced.co.uk/pru.shtml?spk7wglu.htm)	RRID:SCR_000903
G*Power	http://www.gpower.hhu.de/	RRID:SCR_013726

CONTACT FOR REAGENT AND RESOURCE SHARING

Further information and requests for resources and reagents should be directed to and will be fulfilled by the Lead Contact, Barry Dickson (dicksonb@janelia.hhmi.org).

EXPERIMENTAL MODEL AND SUBJECT DETAILS

Flies were raised on power food [39] at 50% relative humidity and 25°C, or 29°C for cell killer experiments (ablation of aSP22 verified by immunostaining, showing no remaining *GAL4*-positive neurons in 6 of 6 hemispheres). Lights were off 8pm-8am, except for flies for CsChrimson experiments, which were dark-reared on food containing 0.2mM all-trans retinal (Toronto Research Chemical, #R240000). Behavioral experiments were performed between 3-7pm, 3-7 days after eclosion, at 25°C, 40% humidity. Electrophysiology experiments were conducted 2-3 days after eclosion. When needed before experiments, anesthesia was performed on ice. Fly strains were a gift of Barret Pfeiffer, Heather Dionne and Gerald Rubin [16–18] except where specified. Wild-type: Canton S. Driver lines (used as described in figure legends, or below) were: *GMR22G01-GAL4* in *attP2*, aSP22 split GAL4 *aSP22-SS1*, and aSP22 split GAL4 *aSP22-SS2*. Effector lines used were: *10XUAS-IVS-mCD8::GFP* in *su(Hw)attP5* (pJFRC2) (Figures 1D, S1A, and S1J–S1M), *UAS-sytGFP* (Bloomington Stock Center #6925) (Figures 1E–1H, pseudo-colored magenta), *pJFRC22-10xUAS-myr::tdTomato* in *attP2* (Bloomington #32221) (Figures 1E–1H, pseudo-colored green), *20XUAS-CsChrimson-mCherry* [20] in *su(Hw)attP5* (aSP22 behavior and electrophysiology), *UAS-DTI* [34, 35] (Figures 1B, 1C, 1M–1O, and S2B–S2E), *pBPhsFlp2::PEST in attP3;; pJFRC201-10XUAS-FRT>STOP>FRT-myr::smGFP-HA in VK00005,* and *pJFRC240-10XUAS-FRT>STOP>FRT-myr::smGFP-V5-THS-10XUAS-FRT>STOP>FRT-myr::smGFP-FLAG* in *su(Hw)attP1* for multicolor flipout stochastic labeling [36] (Figures 1D and S1C–S1I). All transgenes were in a w^{1118} background. Tests were performed on heterozygotes. Behavior and electrophysiology experiments used flies with a wild-type X chromosome to permit normal vision. Controls omitted either the *GAL4* driver or the *UAS* effector; for example, for the *aSP22-SS1>DTI* experiments, controls were *aSP22-SS1* with no *UAS-DTI* ("*aSP22-SS1* control") and *UAS-DTI* with no *aSP22-SS1* ("*DTI* control").

METHOD DETAILS

Identification of aSP22 neurons

GAL4 driver lines [16, 17] were screened for neurons projecting from higher brain regions to motor areas for the body parts involved in courtship actions. One line (*GMR22G01-GAL4*) targeted, among other cells, a descending neuron pair from the dorsal brain (Figure S1A), that expresses the courtship-related male Fruitless proteins (Fru^M, Figure S1B). Using our nomenclature for Fru-expressing neurons [40], we designated this pair aSP22.

To target aSP22 more specifically, we refined the expression pattern using split GAL4 intersections [16, 18, 19]. After screening several hundred intersections, we identified two sparse split GAL4 combinations, *aSP22-SS1* and *aSP22-SS2*, that target aSP22 and few additional cells (Figures S1J–S1M). The activation phenotypes of *aSP22-SS1* were all shared by *aSP22-SS2* (Figures 1I–1L) – proboscis extension, abdomen bending and leg movements. If the additional cells are not the same between *aSP22-SS1* and *aSP22-SS2*, the aSP22 neurons themselves could be reasoned to be responsible for the phenotypes common to both lines. Indeed, the additional cells can be seen to lie in different locations in *aSP22-SS1* (Figure S1J) and *aSP22-SS2* (Figure S1K). For confirmation that these additional cells are not the same between the two split GAL4s, we combined the transgenes for each split GAL4 all into the same animals; when the two split GAL4s are combined there should be a higher count of additional cells than in each line alone. This is what we observed (Figure S1N). Furthermore, while aSP22 was always labeled, the additional small cells were not labeled in every hemisphere (Figure S1N) and so are unlikely to be responsible for the observed phenotypes with high penetrance (Figure 3D).

We further note that in the split GAL4 flies, the only cells besides aSP22 are found in the brain, not the ventral nervous system, therefore decapitated flies have only the descending arbors of aSP22 and no other cells. In those flies, activation successfully elicited abdomen bending and foreleg movements (Figures 3B and 3C), so these actions can be definitively attributed to aSP22.

Immunohistochemistry and image processing

Staining and imaging were performed using published methods [36]. Images were collected at 20x. For multicolor flipout, flies received a 15min heat shock at 37°C at 1-3 d old, and were dissected at 6-8 d. All other staining experiments were performed on 3-7 d old flies. Antibodies used: rabbit anti-GFP (1:500, Thermo Fisher Scientific, Waltham, MA, #A11122), rabbit anti-Fru^M [33], chicken anti-GFP (1:2000, Abcam, Cambridge, MA, #ab13970), mouse anti-nc82 (1:50, Developmental Studies Hybridoma Bank, University of Iowa), rabbit anti-DsRed (to detect tdTomato; 1:1000, Clontech Laboratories, Inc., Mountain View, CA, #632496), rat anti-flag (Novus Biologicals, LLC, Littleton, CO, #NBP1-06712), rabbit anti-HA (Cell Signaling Technology, Danvers, MA, #3724S), mouse anti-V5 (AbD Serotec, Kidlington, England, #MCA1360), AlexaFluor-488 (1:500; goat anti-rabbit, goat anti-chicken, goat anti-mouse; Thermo Fisher Scientific), AlexaFluor-568 (1:500; goat anti-mouse, goat anti-rat; Thermo Fisher Scientific), AlexaFluor-633 (1:500; goat anti-rat; Thermo Fisher Scientific).

Images were adjusted for gain and contrast in Photoshop without obscuring data. Where noted, brain images were registered using the Computational Morphometry Toolkit (http://nitrc.org/projects/cmtk) [37] with a male template brain (JFRC2014) corrected by a z scaling factor of 1.568 to match the true proportions of a fly brain [41]. To score dimorphism in neuronal arbors, Fiji software (http://fiji.sc/) was used to equalize and binarize multicolor flipout images and analyze volumes. neuTube software [38] was used for neuronal tracing (Figure 1D).

CsChrimson activation

Behavior was filmed with Basler A622f cameras at 30 Hz, controlled by gVision software developed at Janelia (Gus Lott). The CsChrimson stimulus light was a 656 nm LED spotlight (Mightex PLS-0656-101-C) controlled through a NIDAQ board and Labview software (National Instruments, Austin, TX). An 880nm infrared LED (Fairchild Semiconductor Corporation #QEE123) was connected to a fiber optic in the field of view, to indicate when the stimulus was on, since a longpass 830 nm filter in front of the camera prevented the stimulus light from obscuring the behavior video. Ambient lighting was provided by two infrared security spotlights (Phenas). Each stimulus was 2 s of constant light, with 20 s interstimulus intervals. In open-field assays, flies were filmed in cylindrical acrylic chambers, 3 mm high x 9 mm in diameter. In decapitation assays, heads were cut off with razor blades and flies tested 10 min later, standing upright on a surface, not tethered. Flies that could not stand were discarded. For tethered flight assays, each fly was waxed by the thorax to a pin with an Electra Waxer (Almore International). In tethered flies, there is no female present, so leg lifting latency was therefore scored in tethered flies as the frame in which both forelegs are furthest extended in front of the head, toward where a female would be during courtship.

Courtship

Courting pairs were filmed from both below and above (at resolutions of 208x208 and 164x164 pixels) in cylindrical acrylic chambers, 9 mm diameter x 3 mm high, with a divider keeping flies apart until the start of the assay, and a white LED ring light around the chamber. All females used in courtship assays were Canton S virgins. Males were reared in isolation for courtship. Flies were loaded into chambers without anesthesia and were filmed for 30 min. Behaviors were scored for the 30 s after the first wing extension, except copulation, which was scored within the 30 min window. Scoring was performed manually using VCode software (http://social.cs.uiuc.edu/projects/vcode.html), switching between top and bottom views when a body part was obstructed in one view. Quantification was performed by two independent observers to validate the scoring (see below). Previous work using manual quantification to detect multiple body parts did not use two cameras or score actions in every frame, which is what leads to our designation of ''high-precision.'' Each behavior was scored separately to avoid implicitly biasing onset time sequences. Proboscis extension and abdomen bending were scored in any frame in which these body parts differed from the resting position. Leg lifting was defined as any frame in which both male forelegs were lifted off the ground toward the female. For an index of following and locomotion in aSP22 > DTI experiments, flies were tracked by machine vision with Matebook software [24]. Following was defined as frames in which the angle between the male and female body axes did not exceed 90°, each had a speed of at least 1 mm/s, and these conditions persisted for at least 0.2 s. From the high-precision manual scoring, latencies for Figure 3E were scored as relative onset times of proboscis extension, abdomen bending, and leg lifting in engagement bouts in which all co-occurred.

For the sequence analysis, a Markov chain analysis identified a behavioral sequence of onset times. The onset times of actions were used to construct an action sequence for each animal, from which a transition matrix was constructed. We considered the null hypothesis that the frequency of transitions from any action A to another action B depends only on the overall frequency at which B is executed among all non-A actions. Statistical significance was determined by permutation tests in which the action sequence was randomly shuffled (n = 10,000). For each permutation, the transition matrix was calculated using Python and hmmlearn (https://github.com/hmmlearn) and compared to the transition matrix from the original sequence. *P*-values represent the proportion of permutations in which shuffled transition probabilities were above the values in the observed transition matrix, with Benjamini-Hochberg multiple testing correction with false discovery rate of 0.1. In analyses in which self-transitions were removed, they were removed from both real and shuffled data before transition matrices were compared; otherwise, the analyses were identical to analyses that included self-transitions.

For analyses in which engagement bouts were defined as overlapping actions (Figures 2I and S3C), self-transitions were excluded, and bouts were defined as continuous series of frames in which at least one engagement action was ongoing, with at least one frame of overlap between different actions. In rare cases (< 10%), the onsets of actions appeared to be simultaneous due to video frame rate, rendering the onset sequence ambiguous; these bouts were omitted from the sequence analysis.

A three-state hidden Markov model was generated and fit to the data (including self-transitions) with the Baum-Welch algorithm using hhmlearn, and the model was used to predict the hidden state at each action onset. The proportions of actions comprising each hidden state are reported in Figure 2E.

To determine whether action onsets were accompanied by co-occurrence of other actions (Figure 3A), "expected": # bout onsets * frequency of other action. "observed": # instances of action onset co-occurring with other action. Each of these plotted as a percentage of total # onsets of that action. Fisher's Exact Test performed on raw values, not percentages. Benjamini-Hochberg multiple testing correction, with false discovery rate of 0.1.

Assessing postural movements

One of the movements that aSP22 activation triggered in the flight assay was an early movement of all legs (Figure 1K; Video S3). Because the legs moved simultaneously in the same direction, this movement might, in a standing fly, trigger a postural change rather than locomotion, which instead uses alternating leg movements. Indeed, in decapitated flies, we found that activating the remaining descending arbor of aSP22 elicited a sexually dimorphic posture change in both split GAL4 lines (Figure S2A). A posture change was scored as positive values if increasing distance from ground. We observed that natural courtship includes previously undescribed postural changes during engagement (both crouching and rising), as the male approaches the female (Video S2). These movements were not quantified in ablation experiments with freely moving, courting flies as they can only be observed during rare instances when the flies are orthogonal to the cameras. We therefore show that aSP22 is sufficient to trigger a postural movement, but tests for necessity are not possible without further assay development.

Feeding

Males were starved approximately 21 hr at 18°C with free access to water, then tethered by waxing the thorax to a rigid surface. 100 mM sucrose or water was presented to the legs from syringe needles as a small droplet, without allowing proboscis contact or ingestion. Water and sucrose were presented five times each, interleaved to prevent receptor desensitization by the sucrose. The fraction of trials in which a fly extended the proboscis in response to sucrose was averaged across flies to give a response rate which was then compared across genotypes by a Mann Whitney U test.

Electrophysiology

Individual flies were anesthetized by cooling. The brain and connected VNS were removed and placed into external saline composed of (in mM) 103 NaCl, 3 KCl, 5 N-tris(hydroxymethyl) methyl-2-aminoethane-sulfonic acid, 10 trehalose dihydrate, 10 glucose, 26 $NaHCO_3$, 1 NaH_2PO_4, 4 $MgCl_2$, 3 KCl, 2 sucrose, and 1.5 $CaCl_2$ (280-290 mOsm, pH 7.3; components from Sigma Aldrich). The connective tissue and sheath were removed using fine forceps and the brain and VNS were transferred to a chamber (Series 20 Chamber, Warner Instruments) superfused with external saline (carboxygenated with 95% O_2/5%CO_2) and held into place via a custom holder. Neurons were visualized using a Zeiss Examiner Z1 with a W N-Achroplan 40X/0.75 water objective, 635 nm LED illumination (pE-4000, CoolLED), and an IR-1000 infrared CCD monochrome video camera (Dage-MTI). Whole-cell recordings were obtained using glass patch electrodes filled with an internal solution composed of (in mM) 140 K-gluconate, 10 HEPES, 1 KCl, 4 MgATP, 0.5 Na_3GTP, and 1 EGTA (270-280 mOsm, pH 7.3, components from Sigma Aldrich) connected to an Axopatch 700B amplifier (Molecular Devices) and digitized (10 kHz) with a Micro 1401-3 using Spike2 software (Cambridge Electronic Design). Glass electrodes were made using a P-1000 micropipette puller (Sutter) from borosilicate glass (Sutter; 1.2 mm outer diameter, 0.69 mm inner diameter). The pipette tip opening was less than one micron with a resistance between 5 and 15 MΩ.

aSP22 neurons were recorded in current clamp mode. aSP22 rested near −50 mV and fired few spontaneous action potentials. If necessary, current was injected to hold the membrane potential near −50 mV while conducting light intensity dose-response experiments. CsChrimson-expressing aSP22 neurons were excited by a constant-on 2 s, 635 nm light pulse delivered every 60 s through the objective. This stimulus replicated that used in behavior experiments. Light intensity presentation order was varied from experiment to experiment; there is no indication that the order of presentation affected responses.

Spikes were identified and counted using Spike2 scripts, and verified via manual inspection. Spiking characteristics were analyzed in detail at the three light intensities that best approximated those examined in behavior latency analyses based on the approximation that 10% of 635 nm light penetrates the *D. melanogaster* cuticle (Figures 4B and 4D–4F) [29]. Total spike counts (from stimulus onset), frequency (from stimulus onset), and instantaneous frequency (1/spike $time_x$-spike $time_{x-1}$) were binned into 1 ms bins to average the data across individuals over time (Figures 4D–4F). The mean latencies to the onset of proboscis extension, abdomen bending, and leg lifting at each intensity (50 μW/mm^2: 261, 560, 880 ms; 150 μW/mm^2: 102, 377, 493 ms; 250 μW/mm^2: 72, 237, 339 ms, respectively) were used as the time points at which spiking characteristics were compared across latencies and intensities. Statistical comparisons were made using a two-way ANOVA (intensity, latency) and post hoc Holm-Sidak pairwise multiple comparisons test (SigmaPlot 12.5). Figure 4D, no significant differences across intensities within a behavioral latency type (e.g., proboscis extension); significant differences across all behavior latency types within an intensity. P: proboscis, A: abdomen, L: legs. P1-A1: $p = 0.002$; P1-L1: $p < 0.001$; A1-L1: $p < 0.001$; P2-A2,L2: $p < 0.001$; A2-L2: $p = 0.02$; P3-A3,L3: $p < 0.001$; A3-L3: $p = 0.007$. Figure 4E, significant

differences across intensities within a behavioral latency type. A1-A2: p = 0.026; A1-A3: p < 0.001; L1-L2: p = 0.04; L1-L3: p < 0.001; L2-L3: p = 0.028; significant differences across behavior latency types within an intensity. P2-A2: p = 0.004; P2-L2: p = 0.001; P3-A3: p = 0.001; P3-L3: p < 0.001. Figure 4F, significant differences across intensities within a behavioral latency type. P1-P3: p = 0.023; A1-A2: p = 0.015; A1-A3: p < 0.001; L1-L2: p = 0.031; L1-L3: p < 0.001; L2-L3: p = 0.028. Significant differences across behavior latency types within an intensity. P2-A2: p = 0.007; P2-L2: p = 0.008; P3-A3: p = 0.004; P3-L3: p = 0.001.

Light intensity calibration

The LED stimulus was delivered (with or without stacked 2.0 and 1.0 neutral density filters in the beam path) through the objective. The aSP22 soma was in the center of the objective field of view, and thus, in the center of the focused LED beam. The LED beam size was calculated using a beam profiler (WinCamD-UCD12, DataRay) with the sensor placed at the approximate distance from the objective as the sample during experiments (2 mm). This yielded a $1/e^2$ beam area of 0.95 mm^2. Light power was measured using a ThorLabs PM100D Compact Power and Energy Meter with a Console S130C Slim Photodiode Power Sensor placed 2 mm away from the center of the objective. In an effort to measure the light power of the focused beam and reduce the amount of unfocused or reflected light from being measured by the 70.88 mm^2 power meter sensor, a painted black foil sheath was placed over the large sensor with an opening for the objective to deliver light. Intensity was calculated as the raw light power measured divided by the 0.95 mm^2 focused beam area.

Logistic regression model

In Figures 4G and 4H, we modeled the link between aSP22 spiking activity and each engagement behavior with a nonlinear logistic regression model. This model assumes that the probability of a behavioral action being observed at time t is given by

$$P(y_i(t)=1)=\frac{1}{1+e^{-\beta_i(a_i(t)-\theta_i)}},$$

where $i=1,2,3$ indexes one of the three behavioral elements in the engagement sequence {1: proboscis extension, 2: abdomen bending, 3: leg lifting}, $y_i(t)=1$ indicates that the i^{th} element of behavior is active at time t, β_i parameterizes the steepness of the threshold function for the i^{th} element of behavior, θ_i is the corresponding threshold, $y_i(t)=0$ indicates that the i^{th} element of behavior is inactive at time t, and $P(y_i(t)=0)=1-P(y_i(t)=1)$. We modeled the accumulation variables, $a_i(t)$, as exponentially smoothed traces of aSP22 spiking activity

$$a_i(t)=\int_{-\infty}^{t} dt' e^{-(t-t')/\tau_i} s(t'),$$

where τ_i is the time constant of the exponential filter corresponding to the i^{th} element of behavior and $s(t)$ is the aSP22 spike train. Because aSP22 activity and behavior were not measured simultaneously, we fit the model to a surrogate dataset that combined examples of aSP22 spiking activity and engagement behaviors in all possible combinations. With neuronal recordings from 5 aSP22 neurons and behavioral measurements from 20 individual flies, this provided 100 = 5*20 surrogate pairs. To perform the fit, we discretized time into 1 ms bins, assumed that $y_i(t)=0$ for times less than the behavioral latency, and assumed that $y_i(t)=1$ for times between the behavioral latency and the end of the 2 s trial. We also assumed that all three behaviors were statistically independent. To estimate the parameters, $\{\tau_1,\beta_1,\theta_1,\tau_2,\beta_2,\theta_2,\tau_3,\beta_3,\theta_3\}$, we used a maximum likelihood procedure that numerically maximized the probability of the surrogate data over a discrete set of candidate parameters. In particular, we assessed model parameters with two sequential grid searches. We first scanned over parameters coarsely to identify the portion of parameter space that fit the data well. This scan covered $\ln\tau_i\in[-5,5]$ in increments of 0.5, $\ln\beta_i\in[-4,4]$ in increments of 1, and $\theta_i\in[0,75]$ in increments of 2.5. The maximum likelihood parameters resulting from this grid search were $\ln\tau_1=-1.5$, $\ln\beta_1=-2$, $\theta_1=0$, $\ln\tau_2=0$, $\ln\beta_2=-3$, $\theta_2=27.5$, $\ln\tau_3=-1$, $\ln\beta_2=-2$, and $\theta_3=35$. We then performed a tighter grid search over a portion of parameter space where we found high likelihoods. In particular, we scanned $\ln\tau_i\in[-1.5,-0.5]$ in increments of 0.1, $\ln\beta_i\in[-3,-1]$ in increments of 0.25, and $\theta_i\in[0,45]$ in increments of 1. This improved the fit and resulted in the final set of estimated parameters that we plotted in Figures 4G and 4H: $\ln\tau_1=-1.5$, $\ln\beta_1=-1.75$, $\theta_1=3$, $\ln\tau_2=-0.7$, $\ln\beta_2=-2.5$, $\theta_2=22$, $\ln\tau_3=-0.8$, $\ln\beta_3=-2.5$, and $\theta_3=42$. Although the best-fit model parameters indicate that action times are generated stochastically from aSP22 spiking activity, aSP22 spiking activity and behavioral responses were measured in separate animals, and much of this stochasticity is likely required to account for trial-to-trial variability in aSP22 activity and behavior.

QUANTIFICATION AND STATISTICAL ANALYSIS

All Mann Whitney U tests were two-tailed. Error bars are standard error of the mean (SEM) except where noted. In all jitter plots (e.g., Figure 1B), horizontal bars represent the mean. Outliers were not excluded. n and other statistical information is provided in each relevant figure legend or STAR Methods section. Significance: *p < 0.05, **p < 0.01, ***p < 0.001, N.S.: not significant. All replicates are biological, testing different flies, not retesting the same individuals as technical replicates, with the exception that Figure 1C includes technical replicates (five trials per fly, averaged to give one value, which was then averaged across 30 flies/genotype for biological replicates). Power analysis was performed in G*Power software using an alpha error probability of 0.05 and a power level

of 0.8 to select sample sizes for behavioral experiments. Adjustments for multiple comparisons were performed where noted. Benjamini-Hochberg multiple testing correction used a false discovery rate of 0.1. Experiments were blinded for scoring by assigning random identifications and only unblinding after all scoring.

An independent observer repeated the scoring for two key behavior figures: the ethogram of wild-type courtship (Figure 2A) and the activation of different behaviors at different aSP22 stimulus intensities (Figure 3D). For the former, the two observers showed correspondences of 92% for the start of events and 91% for the duration of events. For the latter, correspondences were 99% for the presence of proboscis extension, 92% for abdomen bending, and 93% for leg lifting.

DATA AND SOFTWARE AVAILABILITY

The datasets generated and analyzed during the current study are available from the corresponding author on reasonable request. Software is listed in the Key Resources Table.